Evaluation of HRRR Wind Speed Forecast and WindNinja Downscaling Accuracy during Santa Ana Wind Events in Southern California

DAISUKE SETO,[a] CHARLES JONES,[a,b] DAVID SIUTA,[c] NATALIE WAGENBRENNER,[d] CALLUM THOMPSON,[a] AND NATHAN QUINN[c]

[a] *Earth Research Institute, University of California Santa Barbara, Santa Barbara, California*
[b] *Department of Geography, University of California Santa Barbara, Santa Barbara, California*
[c] *Southern California Edison, Irwindale, California*
[d] *U.S. Forest Service, Rocky Mountain Research Station, Missoula Fire Sciences Laboratory, Missoula, Montana*

(Manuscript received 19 January 2024, in final form 31 December 2024, accepted 14 January 2025)

ABSTRACT: Santa Ana winds are dry offshore downslope windstorms, commonly observed during autumn and winter across southwestern California in the United States. The accuracy of real-time Santa Ana wind forecasts is crucial for wildfire-related emergency management and decision-making. This research utilizes the U.S. Department of Agriculture Forest Service's diagnostic wind flow model WindNinja (WN) and evaluates 1) the accuracy of 10-m sustained wind speed from an operational coarse resolution mesoscale forecast model and 2) the relative accuracy of high spatial resolution WN downscaled simulations during six Santa Ana wind events. NOAA High-Resolution Rapid Refresh (HRRR) 6-h forecasts with 3-km grid spacing were used as inputs to WN to downscale sustained wind speeds to 500-m horizontal grids. Validation with weather stations shows that WN improved the overall forecast accuracy by 13%, on average, relative to HRRR forecasts. Improvements were also recorded in 71.6% of all weather stations used. However, overall WN skill scores declined at higher observed wind speeds. HRRR wind speed forecasts have an overall tendency to overpredict at lower observed wind speeds but underpredict at higher wind speeds. Downscaling increased negative wind speed biases of input HRRR forecasts even more at stations located in wind-prone lee-slope canyons. In contrast, stations located at well-exposed ridgetop sites benefitted from downscaling when the stations had negative input HRRR forecast biases, given that the ridgetops were sufficiently resolved in WN.

KEYWORDS: Wind; Forecast verification/skill; Nowcasting; Short-range prediction; Diagnostics; Numerical weather prediction/forecasting

1. Introduction

Santa Ana winds are dry offshore downslope windstorms, commonly observed during autumn and winter across southwestern California in the United States. They are synoptic-forced mesoscale winds originating from a higher pressure air mass over the Great Basin and the upper Mojave Desert relative to the air mass over the coast (Raphael 2003; Hughes and Hall 2010; Jones et al. 2010). The strong downslope winds associated with these events are produced from gravity waves that develop as statically stable air is driven westward over the mountains of Southern California due to a midtropospheric pressure gradient (Durran 2003; Hughes and Hall 2010). There are also local thermodynamic contributions when gap winds form due to large temperature gradients between cold desert surface and relatively warm overocean air at the same altitude (Hughes and Hall 2010). Gravity waves are transverse waves that develop due to vertical differences in air density. If an air parcel in stably stratified flow is displaced vertically, the buoyancy force will accelerate the parcel back toward its equilibrium position. The air parcel will overshoot, however, and oscillate about the equilibrium level, producing waves at the Brunt–Väisälä frequency (Durran 1990). Gravity waves induced by flow across mountain barriers are referred to as "mountain waves." Hydraulic theory is often employed to explain the formation of strong downslope winds during mountain-wave events and is perhaps the most widely accepted model (Durran 1990). Hydraulic jumps characterized by very strong downslope winds have been previously identified during Santa Ana events (Cao and Fovell 2016). The downslope winds that develop from mountain waves occur in many locations throughout the midlatitudes. Examples outside of Southern California include the Alpine foehn, Rocky Mountain chinook, and the Croatian bora wind.

Hot, dry, and gusty weather conditions associated with adiabatic warming and drying during Santa Ana wind events have contributed to powerline-caused ignitions and rapid fire spread when the vegetation is very dry. The spatiotemporal characteristics and intensity of downslope winds during each Santa Ana event are different, but the highest wind speeds typically occur on lee slopes as the relatively colder, denser air accelerates down toward the coast and warms adiabatically (Cao and Fovell 2018). The fast-moving cold air drains from the desert toward the coast and accelerates through mountain gaps and passes and also in the constriction between the

Denotes content that is immediately available upon publication as open access.

Supplemental information related to this paper is available at the Journals Online website: https://doi.org/10.1175/WAF-D-24-0013.s1.

Corresponding author: Daisuke Seto, d_seto@ucsb.edu

DOI: 10.1175/WAF-D-24-0013.1

mountain tops and the overlaying inversion. Reduced pressure within the accelerated flow upsets the hydrostatic balance, causing the upstream air to hug the slope and accelerate on the lee slope (Stull 2011; Rolinski et al. 2019).

The accuracy of real-time Santa Ana wind forecasts is crucial for fire spread modeling, smoke transport, and emergency management decision-making. Therefore, several model verifications of Santa Ana wind events have been done. Cao and Fovell (2018) examined the skill of high-resolution Weather Research and Forecasting (WRF) Model wind forecasts at 667-m grid spacing using a dense network of near-surface wind observations (~324 stations) in complex terrain during six Santa Ana wind events in San Diego County in Southern California. They found that even though network-averaged wind forecast bias was found to be nearly zero, the model tended to overpredict wind speeds where observed winds were relatively light and underpredict at the windiest sites. Fovell and Gallagher (2018) showed a similar forecast underprediction bias during a strong but localized Santa Ana wind event using high-resolution numerical simulations and wind observations obtained from a network of near-surface weather stations in Ventura County in Southern California.

While Santa Ana winds often impact the broader Southern California coastal region, strong and damaging winds are often localized. Moritz et al. (2010) showed that large spatial variations in the extreme wind pattern can exist during Santa Ana wind events. The high spatiotemporal variability creates challenges for those wishing to maintain situational awareness during Santa Ana wind events (e.g., utilities and fire agencies) and those providing emergency response. Therefore, a high-resolution and rapidly updating wind forecast product is needed to predict such spatiotemporal variability.

Predicting localized high wind events in complex terrain using mesoscale numerical weather prediction (NWP) models requires grid spacing that is small enough to capture local topographic impacts. One example of the need to accurately predict localized high wind events is in support of public safety power shutoff situations when utilities may make decisions to turn off power on the circuit level, which can encompass areas smaller than 1 km^2. However, high-resolution mesoscale modeling in complex terrain typically faces issues such as numerical errors with resolved steep terrain, placement of nesting grid boundaries over complex topography, and feature positional errors associated with limited topographic resolution (Chow et al. 2019). Current PBL schemes used in NWP were also developed from measurements of boundary layers over flat terrain and rely on assumptions that may break down as the topography gets steep (Chow et al. 2013; Siuta et al. 2017).

The U.S. Department of Agriculture Forest Service's WindNinja model (hereafter, WN) is a diagnostic wind model developed to dynamically downscale wind predictions from NWP models (Forthofer et al. 2014). WN is primarily designed to simulate mechanical effects of terrain on the flow, such as ridgetop speedup, flow channeling around terrain obstacles, and reduced speeds in the lee of terrain features. WN can be run at very high spatial resolution (tens of meters) to resolve individual terrain features without significant computational cost (Wagenbrenner et al. 2016). WN can be used to downscale each output time of an NWP model to provide a high-resolution wind forecast. Forthofer et al. (2014) and Wagenbrenner et al. (2016) investigated the ability of the mass-conserving solver in WN to improve near-surface wind predictions in mountainous terrain with topographic variations. They showed that diagnostic downscaling generally improved wind predictions from NWP models and also captured important terrain-induced flow features to improve wildfire spread predictions in complex terrain. These previous downscaling evaluations have focused on high wind periods with near-neutral atmospheric stability over isolated mountains surrounded by fairly simple terrain. Additional evaluations are warranted in more rugged terrain and under other atmospheric conditions. This work provides an evaluation of WN performance under thermally driven downslope windstorm conditions over a relatively wide geographic domain compared to previous studies.

This research verifies WN against a dense surface mesonet to determine its potential applicability as a nowcasting tool under Santa Ana wind events. We focus on nowcasting because predicting extreme wind events developing in localized areas and in short time periods is still a challenge today (Benjamin et al. 2023). The early detection of situations conducive to warnings and the immediate delivery of such information to communities is an essential aspect in nowcasting [World Meteorological Organization (WMO) 2017]. The main research objectives are to examine 1) the accuracy of 10-m sustained wind speed from an operational coarse resolution forecast model and 2) relative accuracy of high spatial resolution WN downscaled simulations. A dense network of wind sensors (~1600 stations) sited in both flat and complex terrain in Southern California was used to evaluate the accuracy of operational forecasts and finer-resolution downscaled wind predictions from WN. Specifically, the accuracy of the operational High-Resolution Rapid Refresh (HRRR) 10-m wind speed forecasts with and without WN downscaling is assessed during Santa Ana wind events.

2. Methodology

a. Santa Ana winds case studies

Six Santa Ana wind events were selected for this study (Table 1) to evaluate the hourly sustained wind speed forecast accuracy of HRRR and WN. These six events capture a range of Santa Ana wind events of varying degrees of spatial coverage and overall magnitude. Each event was issued some form of wind or fire weather product from the National Weather Service with start and end dates providing a general case-study boundary determined by the onset and cessation of winds (Table 1). Observations from Southern California Edison (SCE) mesonet stations were used to evaluate forecast accuracy. Wind events during 2021 and 2022 were chosen to leverage observations from the expanding utility weather station network in Southern California that only recently came into existence. Figure 1 shows observed mean sea level pressure (MSLP) differences between Los Angeles International Airport (LAX) and Daggett-Barstow Airport (DAG), which can be used to evaluate the strength of northeasterly winds during these Santa Ana wind events (see Fig. 3 for airport

TABLE 1. Santa Ana wind case studies, event start and end dates, and the status of the weather alerts issued by NWS Los Angeles forecast office. Note that WA = wind advisory and HWW = high wind warning.

Case No.	Start date	End date	Red flag warning	Wind advisory or high wind warning
1	21 Jan 2022	24 Jan 2022	No	Yes (HWW)
2	18 Jan 2021	21 Jan 2021	Yes	Yes (HWW)
3	20 Nov 2021	23 Nov 2021	Yes	Yes (WA)
4	23 Nov 2021	26 Nov 2021	Yes	Yes (HWW)
5	1 Feb 2022	4 Feb 2022	No	Yes (HWW)
6	14 Oct 2021	17 Oct 2021	Yes	Yes (WA)

locations). The MSLP difference is an important indicator in the identification and forecasting of Santa Ana episodes in Southern California (Sukup 2013; Rolinski et al. 2019; Fovell and Gallagher 2018). Red flag and high wind warnings issued by the National Weather Service (NWS) can also indicate the occurrence of stronger Santa Ana wind events.

The intensity and spatial coverage of the Santa Ana winds at the surface depend on a combination of surface offshore

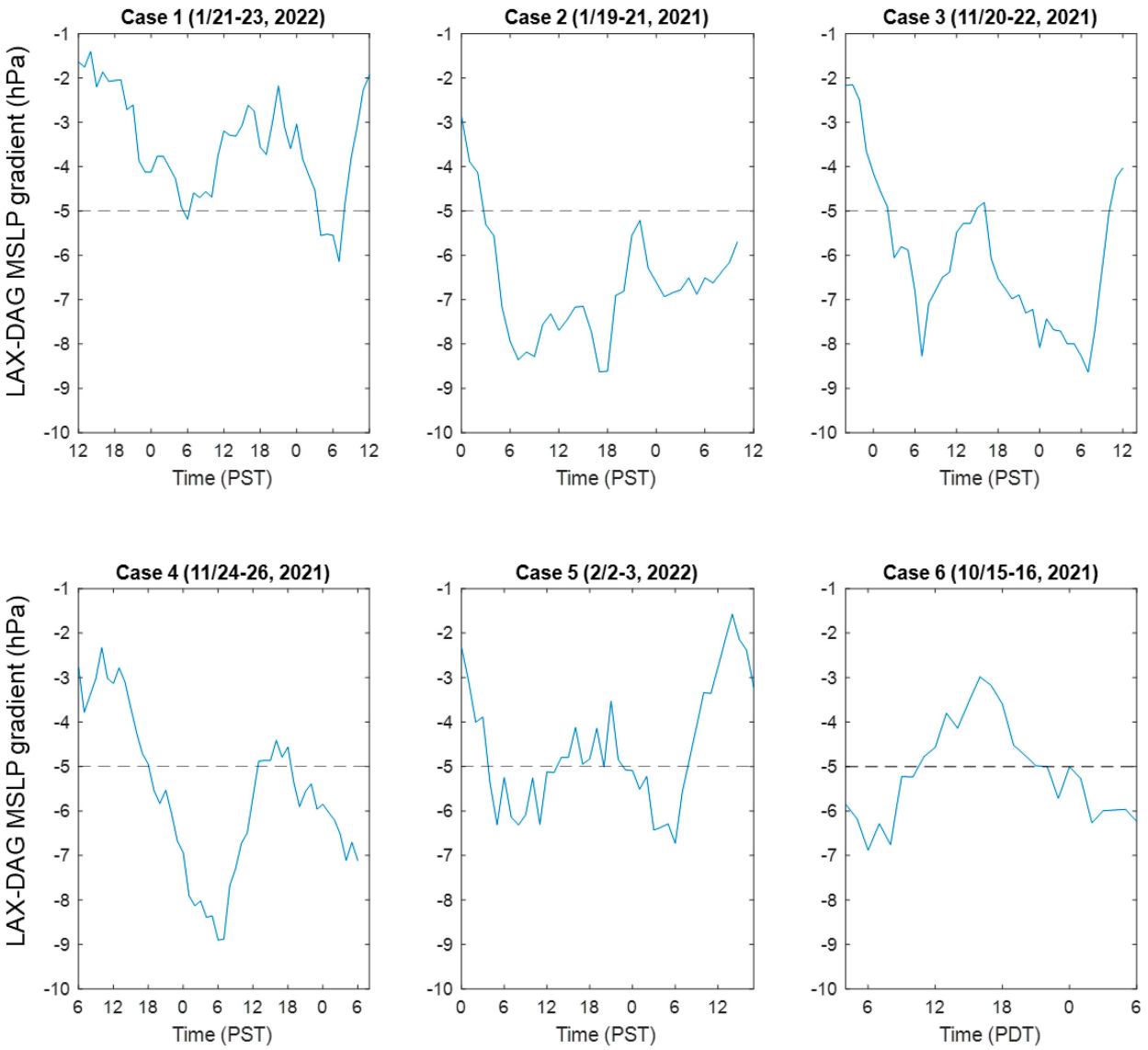

FIG. 1. Time series of hourly MSLP difference between LAX and DAG for the six case studies. The locations of both airports are shown in Fig. 3. Dashed horizontal lines indicate the −5-hPa critical threshold for Santa Ana winds according to NOAA SPC experimental criteria as of April 2024 (https://www.spc.noaa.gov/exper/gradient/).

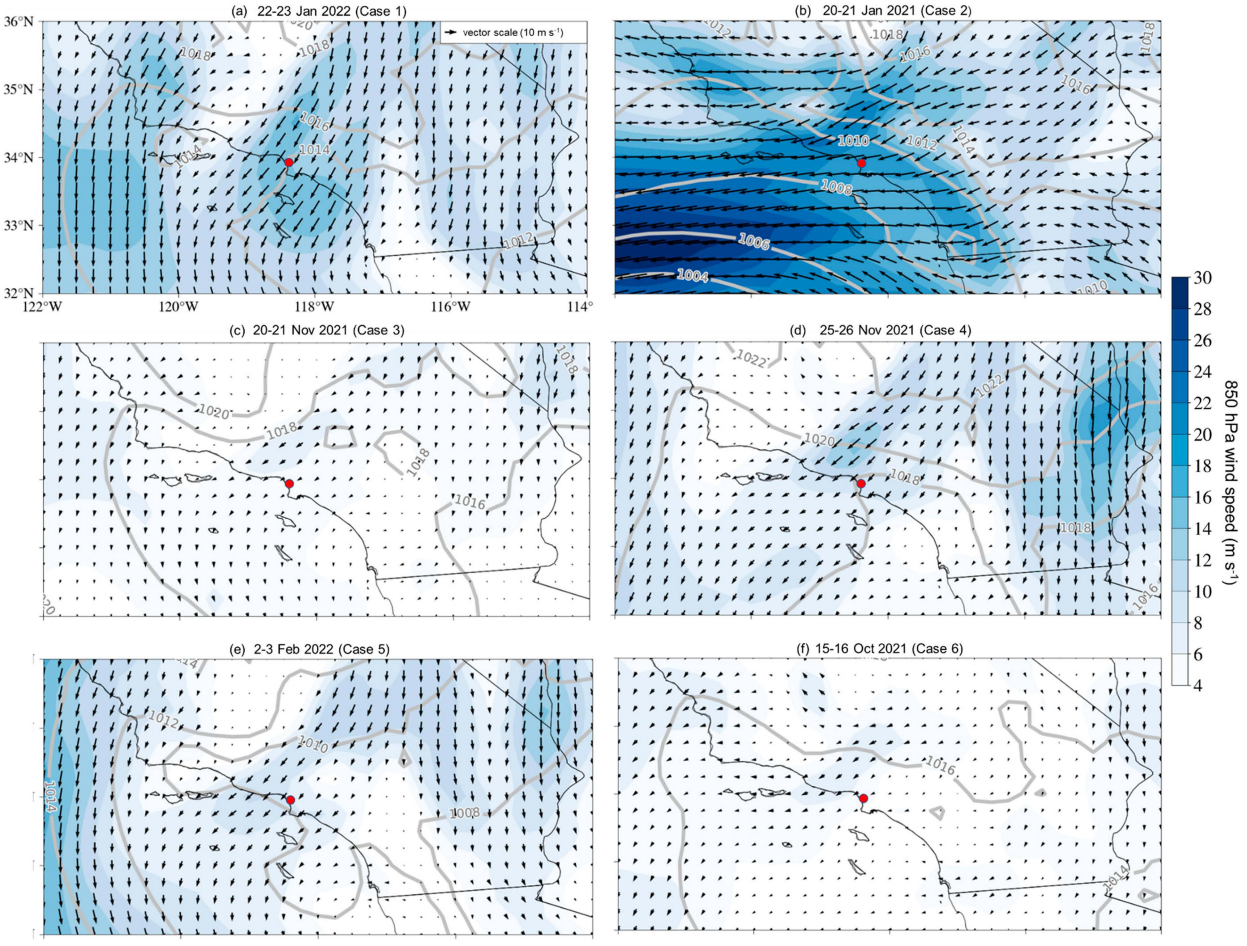

FIG. 2. The 24-h composite (mean of 24 hourly snapshots) of ERA5 MSLP (gray contours; hPa) and 850-hPa winds (vectors; m s^{-1}) over the Southern California domain for each case study shown in Table 1. The MSLP contour interval is set at 2 hPa. The location of LAX is also shown by a red circle marker.

surface pressure gradient magnitudes, wind speed magnitude and direction aloft (e.g., 850 hPa), magnitude of cold air advection in the Great Basin, and anticyclonic vorticity advection at 500 hPa favorable for subsidence (Rolinski et al. 2019). Collectively, these ingredients support offshore flow channeled through mountain passes and lee-slope acceleration/mountain-wave activity. Figure 2 provides the 24-h composite (24 1-hourly images) MSLP and 850-hPa wind speed and direction derived from the ERA5 (Hersbach et al. 2020) for each case study (see Fig. S1 in the online supplemental material for the 24-h composite 500-hPa geopotential heights). While each case was associated with moderate to strong offshore LAX–DAG pressure differences (Fig. 1) of approximately <-5 hPa, the extent and coverage of Santa Ana winds at the surface in each case are different because of differences in the driving synoptic features. For example, cases 1, 2, and 4 are all generally strong Santa Ana wind events because strong offshore winds at 850 hPa accompany the offshore surface pressure differences to help further accelerate winds through the Southern California mountain passes and down lee slopes. Case 2 is notable because of a more easterly wind direction at 850 hPa helping to reinforce surface winds with a more easterly wind direction and generally bringing high winds to areas that typically do not see high winds in most typical Santa Ana wind events (e.g., portions of the Inland Empire west of the Banning Pass that are more subject to high winds when offshore flow arrives out of the east). Cases 3 and 5 are moderately sized events with weaker offshore flow at 850 hPa compared to cases 1, 2, and 4 despite modest offshore pressure differences. The weaker winds at 850 hPa help to limit the spatial coverage of Santa Ana winds. Finally, case 6 is a weaker Santa Ana wind due to modest surface pressure difference and weaker winds aloft (e.g., 850 hPa). The wind direction and magnitude at 850 hPa are also of particular importance to the placement and development of downslope wind conditions with locations downstream of areas where the impinging flow is approximately perpendicular to the mountain range most susceptible to mountain-wave activity and downslope wind conditions.

b. *HRRR forecast model*

The HRRR (https://rapidrefresh.noaa.gov/hrrr/) is the NOAA's operational, hourly updating, convection-allowing forecast model

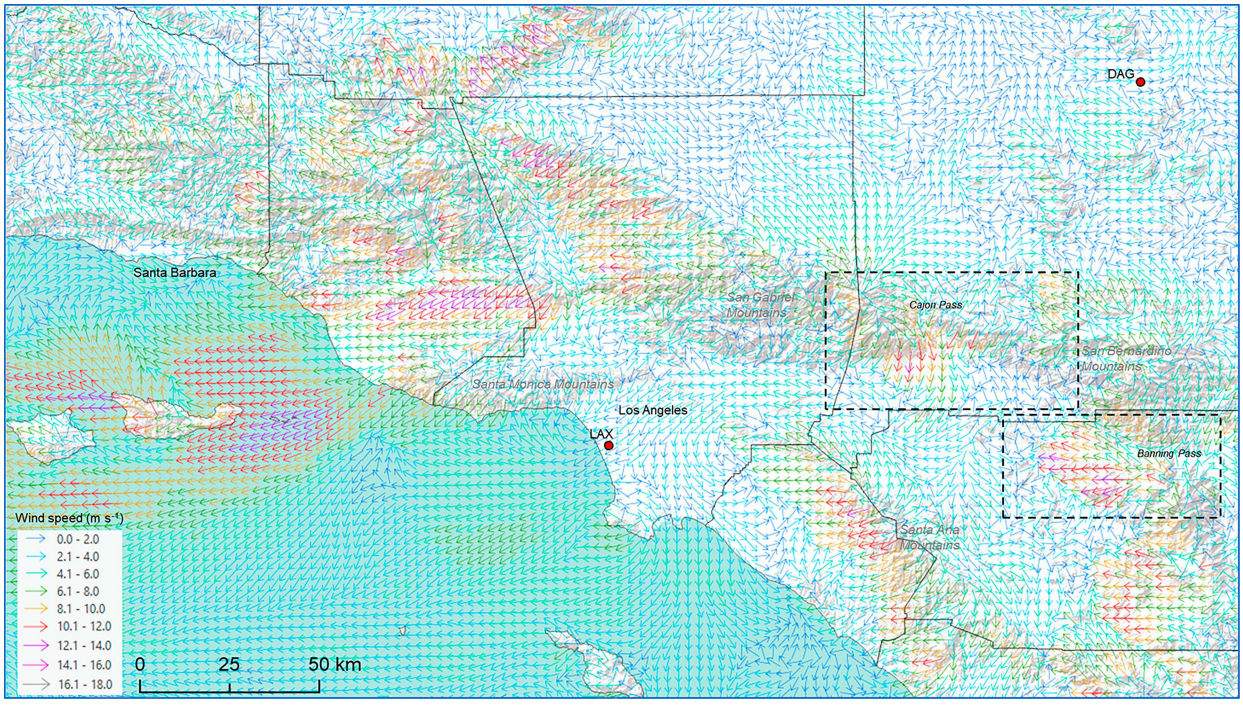

FIG. 3. HRRR 10-m winds forecast during a Santa Ana wind event in Southern California at 0600 PST 22 Jan 2022 (case 1). Topographic features are shown by shaded relief. County borders are shown by solid lines. The locations of LAX and DAG are also shown.

with a horizontal grid spacing of 3 km. The HRRR was developed to provide short-range weather forecasting and situational awareness for high-impact local weather events and rapidly evolving mesoscale weather phenomena, including downslope windstorms and dense smoke plumes from active wildfires (Dowell et al. 2022). Hourly 10-m sustained winds from the HRRR were used as inputs to WN. HRRR data were downloaded from the Amazon web Services website (https://noaa-hrrr-bdp-pds.s3.amazonaws.com/index.html). Figure 3 shows an example HRRR 10-m wind forecast during case 1, and Fig. 4 shows an example WN output for two small regions within the large simulation domain.

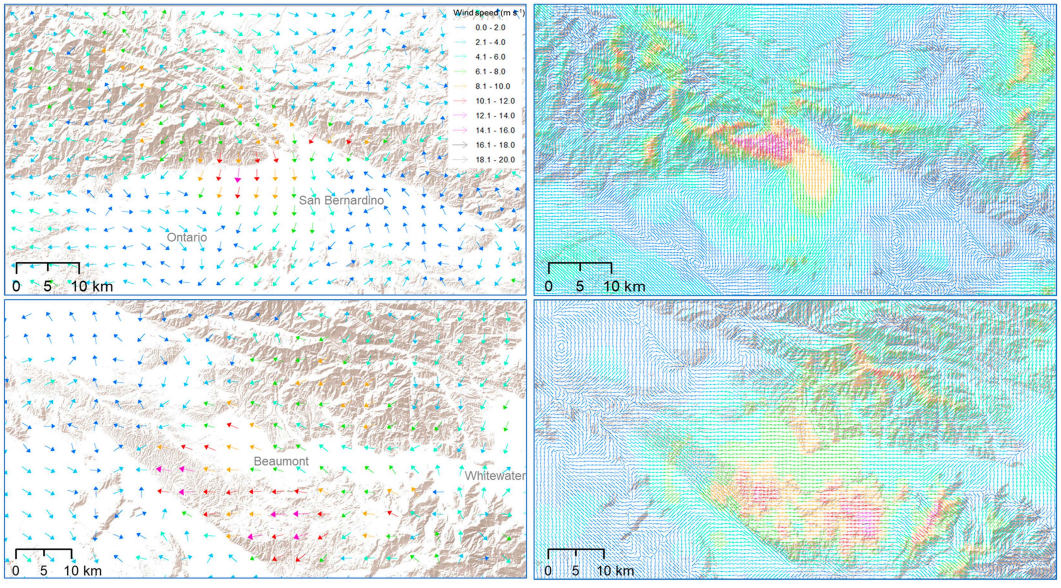

FIG. 4. (left) HRRR and (right) WN 10-m wind forecast for the (top) Cajon Pass and (bottom) Banning Pass shown in Fig. 3 during a Santa Ana wind event in Southern California at 0600 PST 22 Jan 2022 (case 1).

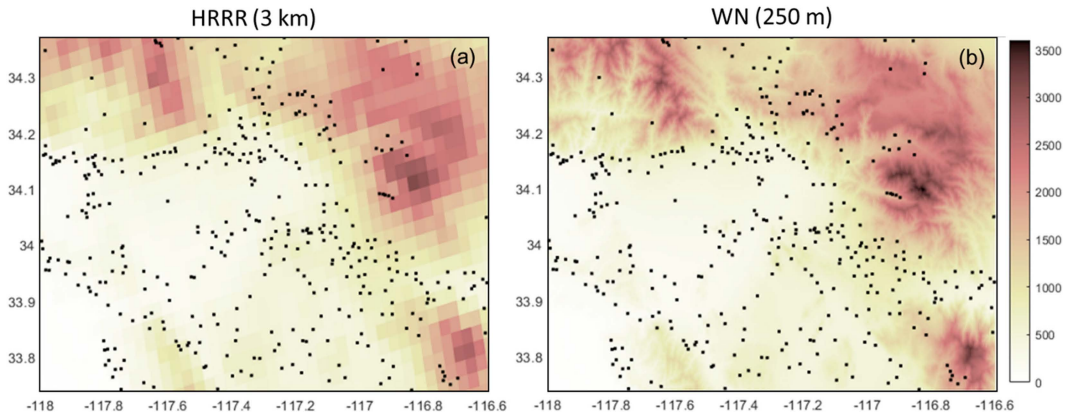

FIG. 5. Terrain representation in (a) HRRR and (b) WN for the area including Cajon Pass and Banning Pass (see Fig. 3 for the area reference). SCE station locations are indicated by dots. Terrain heights are shown with color (meters above sea level).

c. *WindNinja (WN)*

WN is a diagnostic wind model developed to simulate high-resolution winds over complex terrain for operational wildland fire support. WN solves mass and momentum conservation equations to simulate the atmospheric flow accounting for complex terrain features at very high spatial resolution. WN includes simple parameterizations for diurnal slope flow and nonneutral atmospheric stability. The model inputs include terrain elevation, vegetation information, and wind speed and direction. The model can be run in three different ways depending on how the input winds are specified. Input winds can be specified by 1) a coarser-scale weather forecast model, 2) surface wind observations, or 3) a user-specified average wind speed and direction (Forthofer et al. 2014; Wagenbrenner et al. 2016). This research used option 1, such that the WN simulations were predictive in nature allowing for evaluation of a nowcast capability. Specifically, hourly 10-m winds from the first 6 h of each HRRR forecast during the case study period were used as input into WN.

WN has two solver options: 1) conservation of mass and 2) conservation of mass and momentum. The former option is a fast-running solver and calculates a finer-scale wind field by adjusting the initial wind so that the final wind field satisfies conservation of mass. The mass and momentum solver enforces both conservation of mass and conservation of momentum for incompressible, turbulent flows. The mass and momentum solver can provide more accurate wind predictions than the mass-conserving solver in some cases (Wagenbrenner et al. 2019; Forthofer et al. 2014), but it requires much longer simulation times (~60 times slower than the mass solver; Forthofer et al. 2014). Nowcasting operations require fast simulation times to generate a short-term high-resolution forecast. In this case, short term is defined as the next 6 h. To minimize computational time for simulations at high resolution over a large domain, we chose to use the mass-conserving solver in this work. In this study, an initial wind field provided by the HRRR accounts for mesoscale dynamics, which is then downscaled by a higher-resolution wind model to enforce conservation of mass. The domain setup tested in this work was designed around utility operations in Southern California needing to span a large area.

The size of the simulation domain and horizontal mesh resolution also need to be considered, as they affect the total simulation time. The WN computational domain was constructed from 250-m resolution Global Multiresolution Terrain Elevation Data (GMTED). A horizontal grid spacing of 500 m was used in WN to meet forecast generation time requirements for a large Southern California domain (Fig. 3) with the available computational resources. Namely, 6-h forecasts should be able to be generated on the order of 10 min on a standard desktop computer or virtual machine to allow for further processing and visualization of the output for decision-making. The HRRR and WN model terrain plots are shown in Fig. 5.

WN accounts for the effect of vegetation drag on wind flow in a simple way. Users can either specify the dominant vegetation type (grass, brush, and trees) in the WN domain or use a LANDFIRE Landscape file to specify gridded vegetation and elevation information. A spatially uniform "tree" type was selected as the dominant vegetation type for this work. The vegetation is used to set the roughness in the model, which influences the vertical profile of the wind. Model output was requested at 10 m above the vegetation to be consistent with the wind measurement height of the SCE weather station anemometers.

To determine the applicability of WN as an operational nowcasting tool, HRRR 10-m wind forecasts at hourly intervals extending through 6-h horizons were used as input to run WN for downscaling. WN was initialized every 2 h during each event period to create new 6-h nowcast outputs. This approach provides multiple WN output files with 6-h forecast lead time for temporally aggregated average statistics calculations. The thermal parameterizations that simulate diurnal wind and/or nonneutral stability effects were turned off in this work. The diurnal wind model is designed to compute small-scale diurnal slope winds (but not larger-scale diurnal valley winds), and such slope winds should be slight as compared to synoptic- and mesoscale forcing during Santa Ana winds. The nonneutral stability model was also not used as it is not designed to account for mountain waves and downslope windstorms.

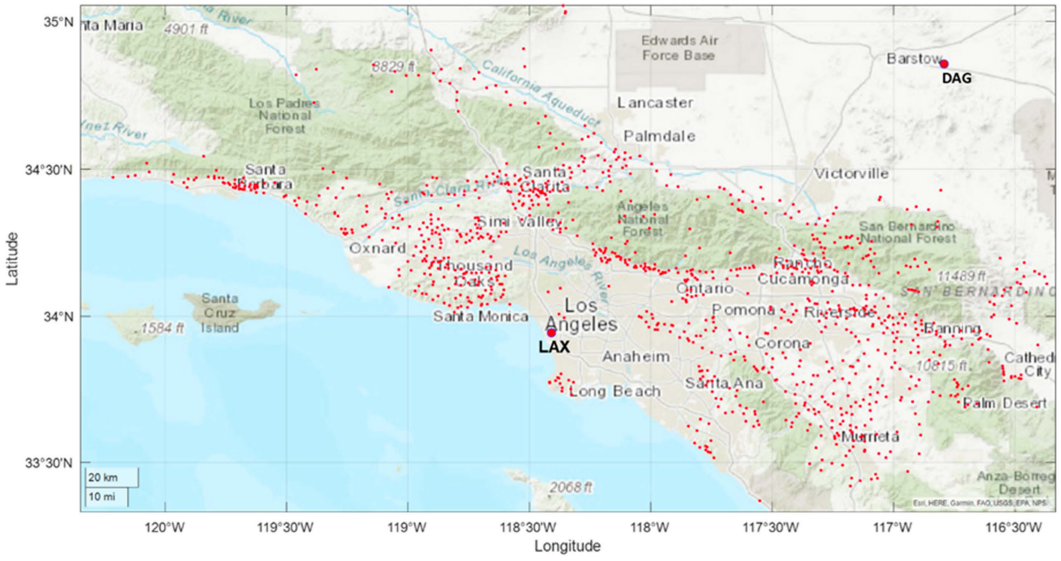

FIG. 6. SCE surface observation locations (red dots). The locations of LAX and DAG are also shown.

The model top height is calculated at run time to be a function of max terrain height and domain extent. The model top height in this study is 10 218 m. The top and lateral boundaries enforce a zero-gradient boundary condition. In this study, an initial wind field provided by the HRRR accounts for mesoscale dynamics (i.e., mountain waves), which is then downscaled by the WN model to account for finer-scale topography. The WN simulation is initialized with only the 10-m horizontal wind components (the w component is initialized to 0) from the HRRR, so the initial wind does not contain a gravity wave signature. A logarithmic profile is assumed in WN to fill in the 3D WN mesh from the 10-m HRRR winds. Since WN does not solve an energy equation, gravity waves cannot form in the WN simulation. A detailed description of the mass-conserving numerical model can be found in Forthofer et al. (2014).

d. Observations

Wind observations from the SCE weather station network were used to compare with nearest gridpoint HRRR and WN outputs. SCE weather stations are installed to monitor real-time weather conditions in high fire risk areas of Southern California, including many Santa Ana wind–prone areas. All SCE stations report sustained winds at approximately 10-m above the ground averaged over a 10-min interval following the WMO guidelines for sustained wind measurement. There were 812 (1006) weather stations in 2021 (2022) within the WN model domain (Fig. 6). SCE observation data are publicly available via the Meteorological Assimilation Data Ingest System (MADIS; https://madis.ncep.noaa.gov) or Mesowest (https://mesowest.utah.edu).

e. Assessment of forecast accuracy

Top-of-the-hour sustained wind speed observations from each SCE weather station were compared against corresponding hourly HRRR forecasts and downscaled WN outputs that were interpolated to sensor locations, using bilinear interpolation. Model performance was evaluated using root-mean-square error (RMSE), mean bias error (MBE), and skill score following Wilks (1995):

$$\mathrm{RMSE} = \sqrt{\frac{1}{n}\sum_{k=1}^{n}(y_k - o_k)^2}, \tag{1}$$

$$\mathrm{MBE} = \frac{1}{n}\sum_{k=1}^{n}(y_k - o_k), \tag{2}$$

$$\text{skill score} = 1 - \frac{\mathrm{RMSE_{WN}}}{\mathrm{RMSE_{HRRR}}} \times 100\ (\%), \tag{3}$$

where y_k and o_k are the model output bilinearly interpolated to the weather station location and observed wind, respectively. Network-, event-, and wind speed bin-averaged statistics were calculated. The relative forecast skill of WN is presented using a skill score, which is often interpreted as a percentage improvement over the reference forecast (input HRRR forecast for WN).

The bin size of the wind speed interval in the histogram analysis presented in this study (see Fig. 10) is selected as 4.47 m s^{-1} (10 mi h^{-1}; mph), with five bins in total. The first (last) bins were defined as the wind speed lower (higher) than 10 (40) mph.

Additionally, categorical verification of HRRR forecasts and WN predictions are considered for forecasts of exceedance of a significant wind speed threshold value. Computation of categorical forecast verification scores can be used to compare the quality of different forecast systems and show to what extent one forecast system give better forecasts than another. We start with a 2 × 2 contingency table (see Table 2) and count the four combinations of yes/no forecasts and yes/no observations [hit (a), false alarm (b), miss (c), and

TABLE 2. A 2 × 2 contingency table used to count the four combinations of yes/no forecasts and yes/no observations. Sustained wind speed of 11.2 m s^{-1} (25 mph) was selected as the threshold value to separate "yes" and "no."

	Observed	
Forecast	Yes	No
Yes	Hit	False alarm
No	Miss	Correct negative

correct negative (d)] for all stations and all forecasting hours. Sustained wind speed of 11.2 m s^{-1} (25 mph) is selected as the threshold value to separate "yes" and "no." This threshold value is also used as part of Red Flag Warning criteria at the NWS Los Angeles forecast office as of April 2024 (https://www.weather.gov/media/lox/QuickReference_public.pdf). The categorical scores calculated by following Schaefer (1990) and Barnes et al. (2007) include

$$\text{probability of detection (POD)} = \frac{N_a}{N_a + N_c}, \tag{4}$$

$$\text{false alarm ratio (FAR)} = \frac{N_b}{N_a + N_b}, \tag{5}$$

$$\text{threat score (TS)} = \frac{N_a}{N_a + N_b + N_c}, \tag{6}$$

$$\text{bias score} = \frac{N_a + N_b}{N_a + N_c}, \tag{7}$$

where N indicates the total number of the event a, b, c, or d. The POD indicates the observed strong wind events that were correctly predicted by the models while the FAR indicates the fraction of predicted strong winds that actually did not occur in the observations. The bias score indicates whether or not the forecast system has a tendency to underpredict (bias score < 1) or overpredict (bias score > 1) strong wind events. The TS can be thought as the accuracy for the quantity being forecast after removing correct "no" forecasts from consideration (Wilks 1995).

3. Results

a. Global statistics

Figure 7 shows the network-averaged skill scores for each case study. The result shows that all skill scores are positive, meaning that WN improved the HRRR forecasts overall. The skill scores do not vary substantially in magnitude over the 6-h forecast lead time. This is because the errors in the HRRR are not increasing significantly over 6 h.

Network- and event-averaged skill scores indicate that the 500-m WN downscaling improved the overall sustained wind speed forecast accuracy by 13% relative to HRRR 3-km forecasts (Fig. 7a). Additionally, Figs. 7b and 7c show that HRRR forecasts have relatively large RMSE and MBE when compared with the observations, even at the time of forecast initialization (forecast lead time = 0 h). This suggests that when WN was run with the configuration chosen here, large initial errors in WN can be traced back to initial errors in the HRRR. Therefore, the accuracy of the initial conditions (i.e., HRRR or other gridded forecast products used for the WN's model initialization feature) is important for the accuracy of WN when configured in the mass conservation approach chosen here, although the errors in WN are not only attributed to those inherited from the HRRR.

The spatial distribution of event-averaged skill scores shows that downscaling with WN improved the forecasts over a majority of stations (71.6% of the stations on average) with respect to reference HRRR forecasts (Figs. 8 and 9). However, the map also reveals that some stations with positive skill scores are located next to station(s) with negative skill scores. It is possible that the HRRR forecast is not providing an optimal "first guess" at the locations where features are smaller than 3 km (local mountain peaks or valleys; see Fig. 5). In these cases, the WN solver attempts to adjust correctly based on the terrain, but it is starting from an initial condition with relatively large errors.

b. Skill scores with wind speed bins

As shown in the previous section, WN improved overall HRRR forecast accuracy over a majority of station locations, as indicated by overall positive skill scores. Figure 10 shows that the positive skill scores were mainly focused on the lower

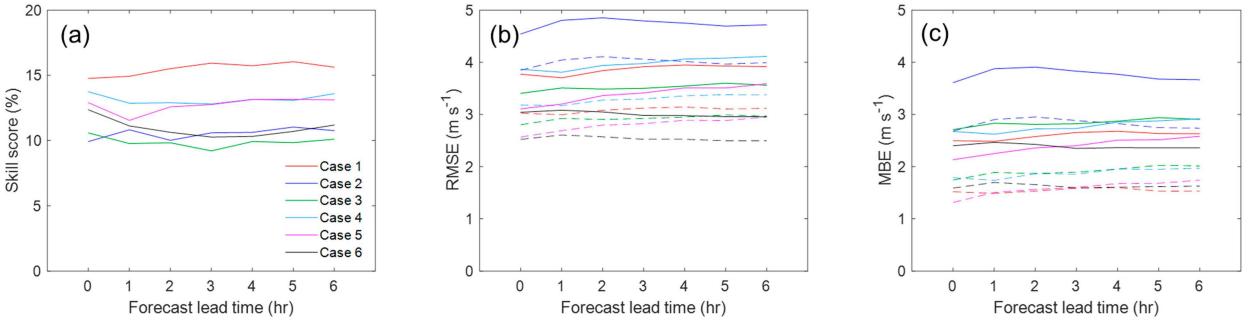

FIG. 7. Network-averaged (a) skill scores, (b) RMSE, and (c) MBE as a function of forecast lead time for each case study. Positive skill scores indicate that improvements in forecast accuracy were made by downscaling HRRR forecasts with WN. The HRRR (WN) statistics are shown in solid (dashed) lines in (b) and (c).

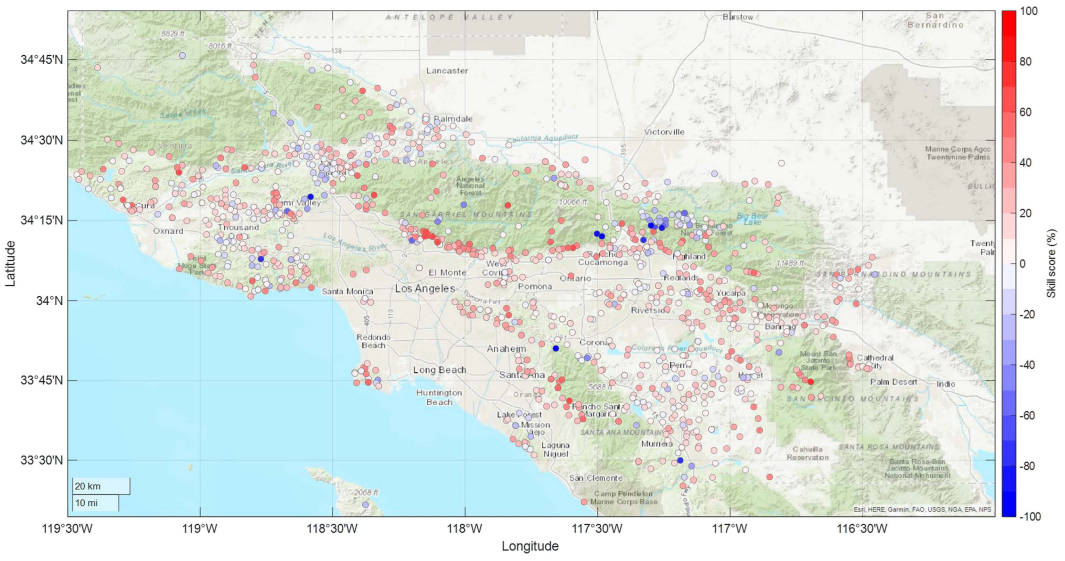

FIG. 8. Spatial distribution of skill scores (%) averaged over all six events. Warm colors indicate that WN improved input HRRR forecasts, whereas cool colors indicate that the input HRRR forecasts were more accurate with respect to downscaled WN predictions.

wind speed bins (<4.5 and 4.5–8.9 m s^{-1} bins). However, downscaling sustained wind speed with WN resulted in a less accurate forecast than the HRRR wind prediction when the observed sustained wind speeds were over 8.9–13.4 m s^{-1} bin. These findings are generally applicable to the individual cases except for case 2. As explained in section 2a, the more easterly wind direction at 850 hPa may have resulted in different terrain interactions than in the other cases, bringing high winds to areas that typically do not see high winds in most typical Santa Ana wind events.

This result is the opposite of what Wagenbrenner et al. (2016) found in their previous validation work. They showed that WN can improve wind predictions by downscaling when input NWP underpredicted wind speeds at ridgetops during high wind events, with the biggest improvements for observed wind speeds over 10 m s^{-1}. However, the Santa Ana winds in this study tend to reach maximum wind speeds on lee slopes of the mountain ranges. The wind flow regime in our study (thermally driven flow under stable atmospheric conditions) was substantially different than in the Wagenbrenner et al. (2016) study (speedup of the wind near the ridgetop under near-neutral atmospheric stability) and likely explains this discrepancy in findings.

There is a substantial atmospheric boundary layer stability effect at play during the strong downslope wind periods of the Santa Ana events. The WN solver is designed to primarily account for mechanically driven terrain effects on flows under neutral atmospheric stability. For strong winds and neutral stability, a speedup of the wind occurs near the top of the mountain along with a turbulent wake on the lee side of the mountain (Stull 1988). In contrast, wind accelerates down the lee side of the mountains during Santa Ana wind events, as a result of strong synoptically forced cross-barrier/mountain winds under statically stable atmospheric conditions. Strong stability and an inversion near the mountain crest level (e.g., San Gabriel,

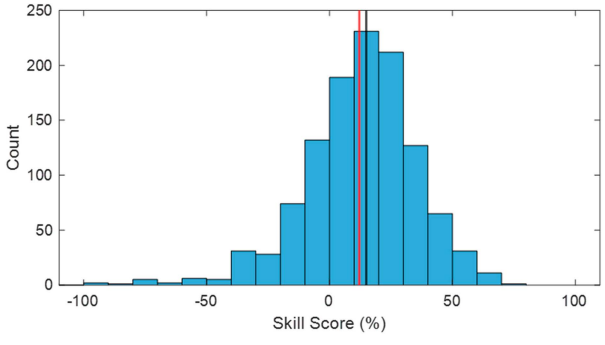

FIG. 9. Histogram showing the frequency distribution of skill scores in the domain in Fig. 8. Red and black vertical lines indicate the mean and median of the distribution.

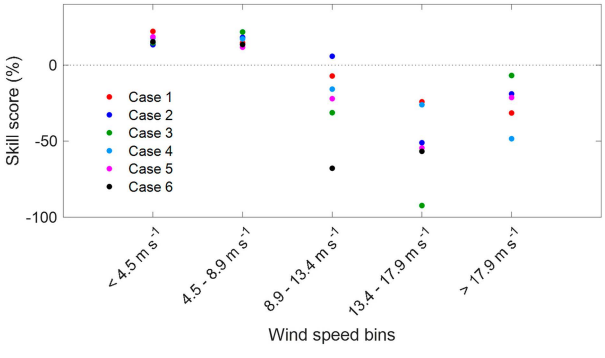

FIG. 10. Network-averaged skill scores (%) aggregated by wind speed bins. Note that observed wind speeds did not reach 17.9 m s^{-1} in case 6.

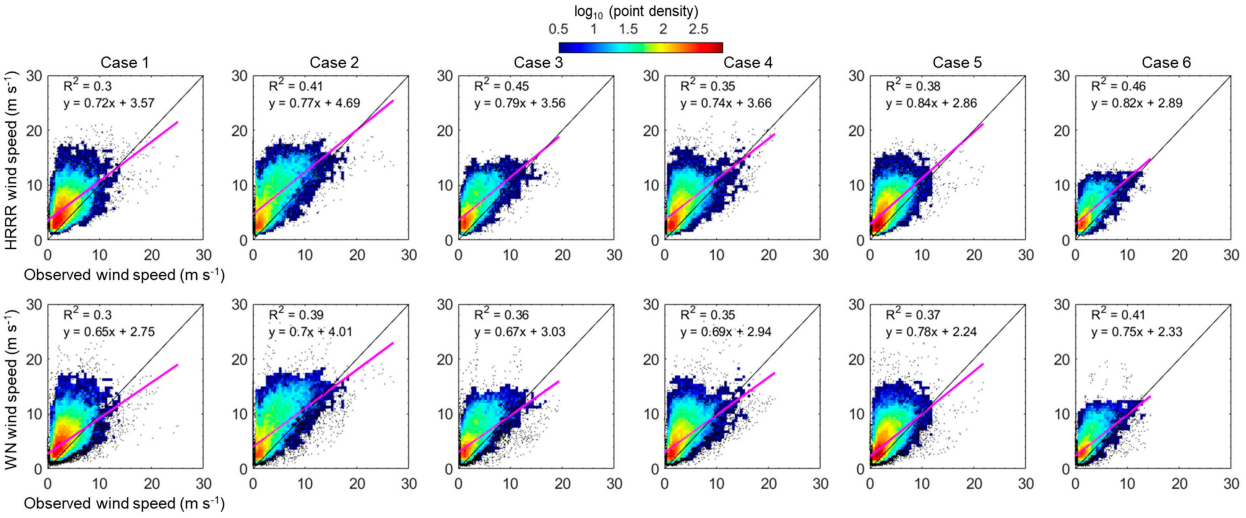

FIG. 11. Scatterplots of observed vs (top) HRRR and (bottom) WN predicted wind speeds for each case study. All hourly observational and forecast data at all locations are plotted together. Color shading indicates point density with logarithmic contour spacing, and the linear regression line for each is shown in magenta. Solid black line is the line of agreement.

San Bernardino, and Santa Ana mountains) associated with the presence of large-scale subsidence on the windward side act as important controls (Barry 2008). The forecast model initialization feature in WN is designed to combine initial mesoscale and synoptic-scale flow fields from a coarse weather forecast with fine-scale flow modifications over complex terrain by WN to provide more accurate wind forecasts. However, when the initial flow fields in the weather model are driven by a statically stable flow regime where winds accelerate on lee slopes, the WN solver lacks treatment of the thermal dynamics driving mountain waves that increase wind speeds on lee slopes. Instead, the WN solver tends to reduce speeds in the lee of terrain features (i.e., WN enforces the mechanical effect of the upwind terrain). Future work could examine the existing thermal parameterizations in WN and possible modifications to them to account for thermally driven downslope windstorms. Due to the nature of extreme wildfire risk associated with intense Santa Ana winds, we examine the trend of decreasing WN skill scores with increasing wind speed in the next section.

c. *Observed versus predicted wind speeds*

All HRRR forecast–observation and WN–observation pairs are presented as a point density heat map for all stations for each case study in Fig. 11. Although there was a lot of scatter both above and below the line of agreement, HRRR regression lines indicate model overpredictions for the lower wind speed range and underpredictions for the higher wind speed range.

Our findings of the overall input HRRR underprediction biases during high wind observations are consistent with Cao and Fovell (2016, 2018) and Fovell and Gallagher (2018). They showed that WRF (2-km horizontal grid spacing) forecast bias (defined as forecast minus observation) is also negatively correlated with the observed wind during a Santa Ana wind event as a result of the model systematically underpredicting at windier locations and overpredicting less windy sites. They found that the forecast sustained wind speed bias is related to horizontal grid spacing and the land surface model and other model physics selections.

WN regression lines fall below the HRRR regression lines for all cases as indicated by the smaller slope and intercept values of WN in Fig. 11. This suggests that downscaling with WN generally has an overall tendency to reduce domainwide wind speeds of input HRRR forecast wind speeds, especially for high wind speeds. This can be broadly explained by the fact that the highest speeds were predicted over the lee slopes during these Santa Ana downslope windstorm events in the HRRR, whereas WN tends to decrease speeds in the lee of terrain obstacles because it is only enforcing mechanical effects. The squared linear correlation coefficients R^2 indicate that the overall spatial structure of the HRRR wind speed predictions were either unchanged or slightly reduced by WN. The intercept values of both HRRR and WN in case 2 are larger than those in other cases, resulting in extended HRRR and WN overprediction biases into higher observed wind speed range. This is because case 2 was the event with a more easterly wind orientation, which perhaps resulted in different terrain interactions (i.e., less effect of downslope accelerations in some areas) than in the other cases.

Figure 12 shows the spatial distributions of HRRR forecast bias when the observed wind speed was greater than 13.4 m s^{-1} (30 mph). Those wind-prone stations indicate that HRRR forecasts tend to underpredict wind speed at many locations.

While network-averaged skill scores were overall negative above 13.4 m s^{-1} as shown in Fig. 10, there were also stations wherein downscaling with WN provided some modest improvement as shown in Fig. 13. Specifically, stations with positive skill scores are located in and near the Banning Pass (cases 1 and 2) and Cajon Pass (case 4). The improvement is likely due to the fact that WN can resolve wind flows in and

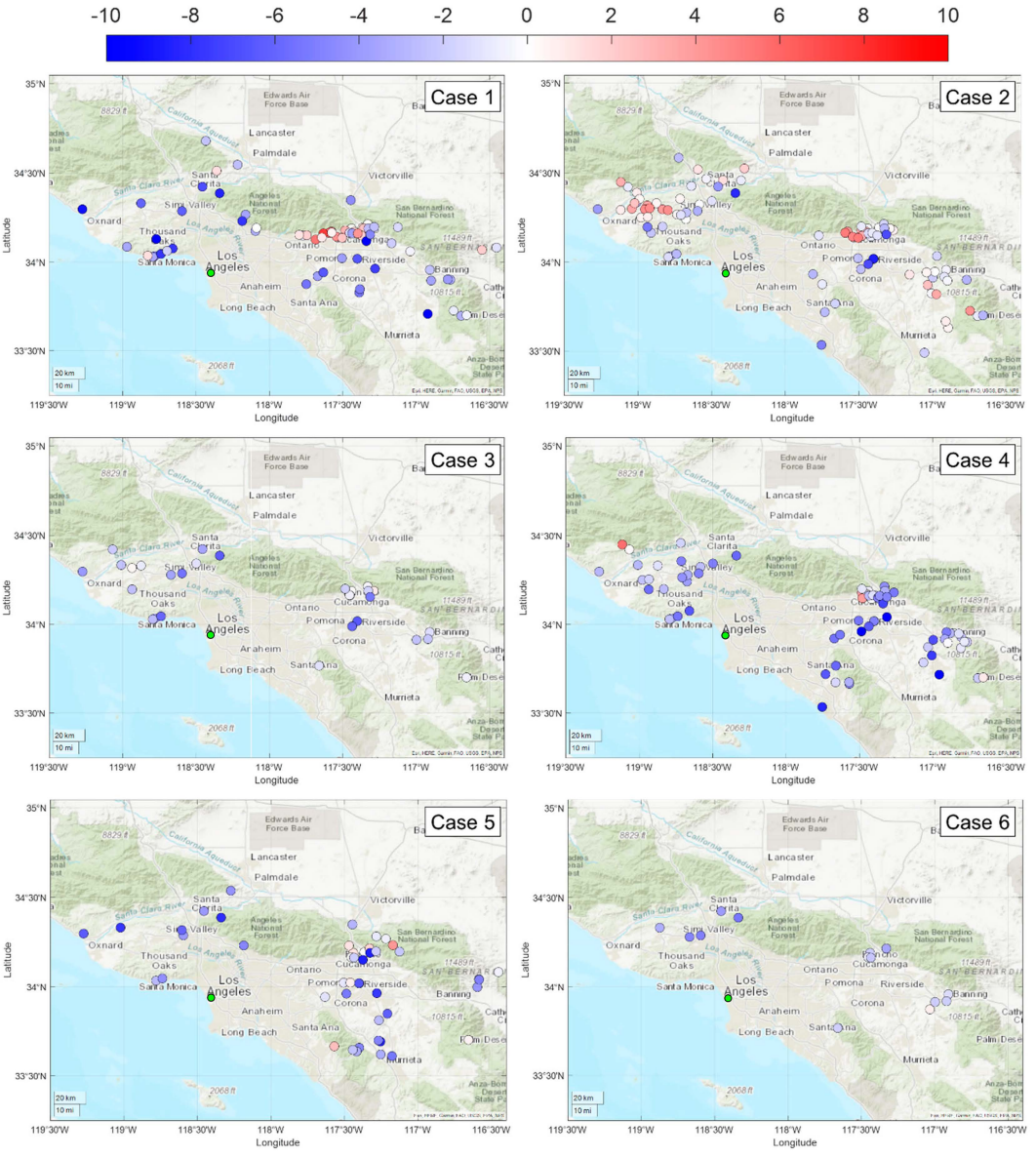

FIG. 12. HRRR model biases (defined as forecast minus observation) calculated when the observed wind speed is greater than 13.4 m s^{-1}. Green dot indicates LAX.

near the gaps that were not sufficiently resolved by the terrain in the HRRR forecast model.

d. Skill scores for ridgetop and canyon stations

In this section, accuracy of HRRR forecast and performance of WN were evaluated for stations located in wind-prone lee slope canyons and on ridgetops within the study domain (Fig. 14). For evaluation purposes, wind speeds below 13.4 m s^{-1} are filtered out from each station. For three selected weather stations sited within wind-prone canyons, WN increased input underprediction biases of HRRR further, resulting in overall negative skill score (Fig. 14; top panels). Although WN reduced the HRRR biases when they were large for the wind-prone canyon sites at some instances, the overall large negative biases persisted after downscaling. For the three selected ridgetop sites, WN reduced the HRRR biases across the entire HRRR bias ranges on the *x* axis and more consistently than for the canyon sites in many cases (Fig. 14; bottom panels). The overall biases remained negative for all ridgetop stations after downscaling.

e. Categorical verification

Figure 15 shows the categorical verification results for each case study. WN resulted in lower POD scores as compared to those of the HRRR for all cases mainly because the total number of Hit counts of WN was lower. This is explained by the fact that downscaling with WN generally has an overall tendency to reduce

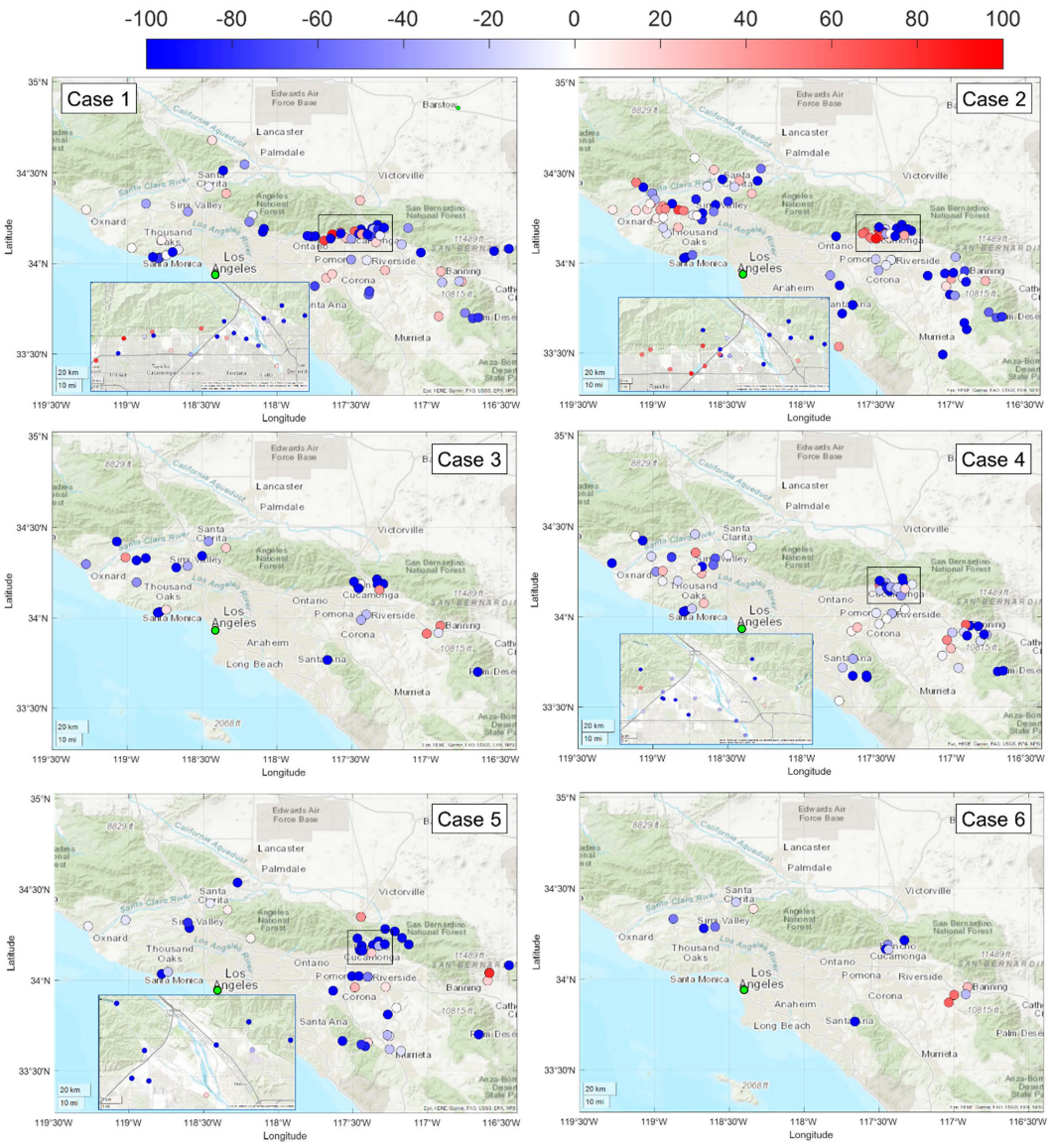

FIG. 13. Skill scores calculated when the observed wind speed is greater than 13.4 m s^{-1}. Warm color indicates that WN improved input HRRR forecasts, whereas cool color indicates that the input HRRR forecasts were more accurate with respect to downscaled WN predictions. Green dot indicates LAX.

domainwide wind speeds of the input HRRR forecast wind speeds, especially for high wind speeds as mentioned in section 3c. On the other hand, the FAR and bias scores were reduced by WN. This result is interesting because WN's overall tendency to reduce the higher wind speed range resulted in overall negative skill scores and lower POD of high wind events. However, WN also reduced the number of false alarm events and bias score due to the tendency of the HRRR model to overpredict wind speeds in locally low-wind areas. TS shows a mixed result, but both HRRR and WN indicate low values, mainly below 0.2.

f. Wind direction analysis

As wind direction and wind speed variations are linked phenomena such as the development and location of downslope winds in complex terrain during Santa Ana winds, analysis of wind direction is also presented in this section. Figure 16 shows observed and predicted wind directions at four selected wind-prone ridgetop and canyon station sites for cases 1, 2, and 3. The results suggest that even though WN can reduce the RMSE of the wind directions, the magnitude of the reductions by WN might be relatively small as compared to the magnitude of the RMSE of the HRRR wind directions for windy locations. The HRRR wind direction predictions can be substantially different than observations even when the observed wind directions are generally unchanged throughout the Santa Ana wind events. Overall, there is no strong evidence that the improved wind speed predictions by WN are linked to the improved wind direction predictions, or vice versa. That will likely

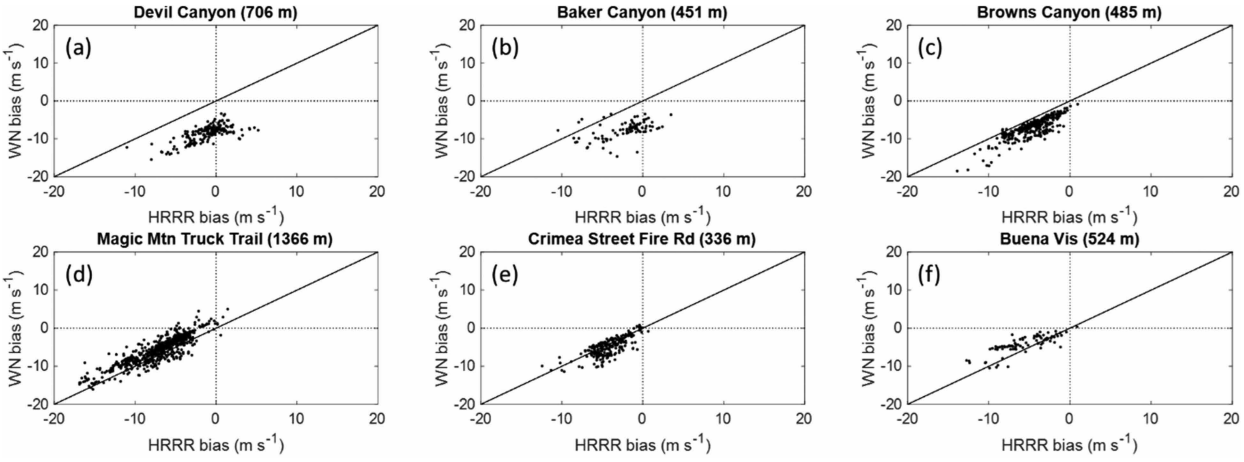

FIG. 14. HRRR forecast bias on x axis vs WN bias on y axis for stations located in (a)–(c) lee-slope canyons and on (d)–(f) ridgetops when observed wind speeds were at or above 13.4 m s^{-1} at the station. The station elevation values are above mean sea level. The observed wind speeds did not reach the threshold values at some locations in some cases. The locations of each station with detailed topography are shown in Figs. S2–S6.

make it difficult to generalize where, why, and how the models are insufficiently representing the actual winds in the entire study domain beyond the overall over- and underprediction biases presented earlier.

4. Modeling considerations for Santa Ana wind events

The WN conservation of mass solver seeks to minimize the change in the initial wind field while adjusting the flow field to conserve mass on a grid that resolves the terrain at a higher resolution than that of the input wind (Forthofer et al. 2014). Initializing with the HRRR, we sought to determine if WN could improve surface wind predictions by accounting for the mechanical effects of the terrain at high resolution while maintaining the larger-scale signature of the downslope wind events. The downscaling results, however, revealed that skill scores decreased, particularly in lee areas, during Santa Ana events. This reduction in skill occurs because the conservation of mass solver only enforces the mechanical effects of the terrain that produces speed up of the flow on the windward and ridgetop locations and reduced speeds in the lee of terrain features. During Santa Ana events, the thermally driven effects dominate over the mechanical effects of the terrain and the highest speeds are observed in the lee of mountain barrier separating the coast from the Mojave Desert and Great Basin. This leeside speedup is a characteristic of a downslope windstorm and is produced from mountain waves that form due to buoyancy-driven effects realized from vertical temperature gradients. Depending on the thermal stratification of the atmosphere at mountain top height and the geometry of the mountain barrier, the flow can get compressed over the mountain and accelerate down the lee side.

The lack of treatment of the thermal dynamics driving these mountain waves is the issue in WN. WN does not solve an energy equation and, apart from two simple thermal parameterizations, does not account for thermally driven flows. The two thermal parameterizations in WN are a diurnal slope flow parameterization based on the shooting flow model in Mahrt (1982) and a parameterization for nonneutral atmospheric stability based on Homicz (2002). Neither of these parameterizations represent the driving dynamics governing mountain waves and downslope windstorm production. Proper representation of these dynamics requires either explicitly accounting for conservation of energy (computationally expensive but plays a critical role in the hydraulic theory thought to govern downslope windstorms during mountain-wave events) or inclusion of a gravity wave parameterization, such as the one described in Barstad (2006) and implemented in Gutmann et al. (2016).

Modeling efforts attempting to better resolve Santa Ana winds must be able to represent these driving dynamics of gravity waves at microscale resolutions. This includes representation of the thermal stratification at mountain top height as well as upwind and downwind of the mountain barrier. Accurate terrain representation is also critical as the height and width of the mountain barrier relative to the Brunt–Väisälä frequency are important controlling factors in downslope windstorm development (Durran 1990). Cao and Fovell (2016) determined that a WRF run at 667 m was able to resolve the hydraulic jump that emerged during a 2013 Santa Ana event. They reported that a WRF run at 2 km was too coarse to produce the jump feature (Cao and Fovell 2016).

Future versions of WN are slated to include a gravity wave parameterization or a conservation of energy equation and could be better posed to handle mountain waves and downslope windstorm dynamics. Work is currently underway to implement a new solver in WN using techniques from fast fluid dynamics to solve the unsteady Reynolds-averaged Navier–Stokes equations in an efficient manner such that an energy equation could be incorporated without substantially increasing model runtimes beyond that of the mass-conserving solver. Diagnostic models giving special treatment to momentum and potential temperature have been shown to simulate

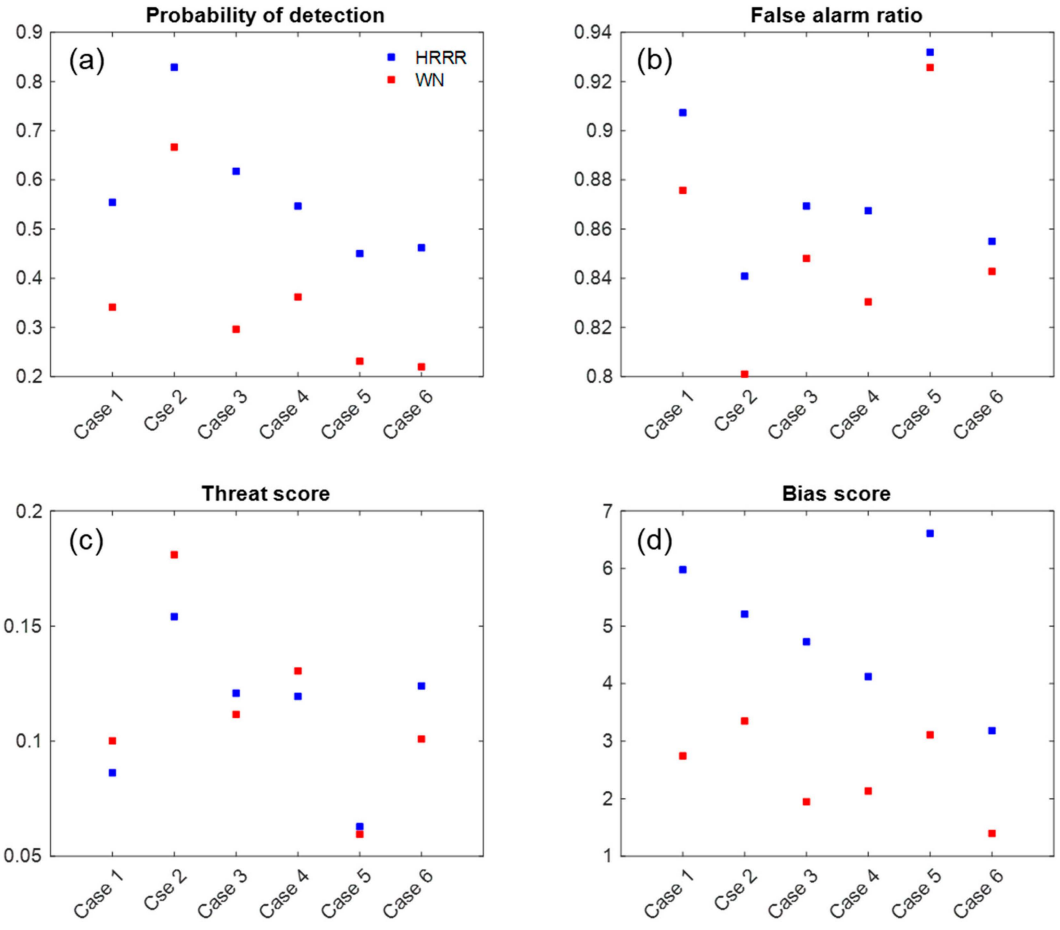

FIG. 15. Network-averaged (a) POD, (b) FAR, (c) TS, and (d) bias score for each case study. The statistics were calculated using the wind speed threshold of 11.2 m s^{-1}.

mountain waves (Onishi 1969; Fosberg 1984); a similar approach could be also explored in WN. Fast-running microscale models will continue to be important for emergency response situations, such as wildland fire. As computing resources improve and new solution techniques are developed and implemented, fast-running models like WN will be capable of simulating the effects of complex atmospheric dynamics at very high resolution under moderate run times on simple hardware.

5. Discussion and conclusions

The accuracy of real-time Santa Ana wind forecasts is important for fire spread modeling, smoke transport, and emergency management and decision-making. This study evaluated the accuracy of NOAA's High-Resolution Rapid Refresh (HRRR) forecasts and the relative forecast improvements by diagnostic downscaling using the WindNinja (WN) model for Santa Ana wind events in Southern California. This study also evaluated WN as a potential diagnostic tool to aid nowcasting operations. The HRRR 6-h forecasts and 3-km grid spacing were used as inputs to WN to downscale sustained wind speeds to 500-m grids. Our principle findings are as follows:

1) WN improved overall forecast accuracy in wind speed by 13% on average against reference input HRRR forecasts by downscaling from 3 km to 500 m during Santa Ana wind events. The improvements were seen for 71.6% of all station locations on average as indicated by overall positive skill scores. However, overall WN skill scores declined to negative values at higher observed wind speed range (observed wind speed $\geq$ 8.9–13.4 m s^{-1} bin), suggesting that WN increased input HRRR forecast errors and biases.
2) HRRR forecasts have relatively large RMSE and MBE when compared with the observations, even at the time of forecast initialization (forecast lead time = 0 h). These errors appear to be the dominant source of error in WN downscaling.
3) HRRR sustained wind speed forecasts have an overall tendency to overpredict at lower observed wind speed range but underpredict at higher wind speed range. WN reduced input HRRR wind speeds across the entire observed wind speed range, resulting in overall positive WN skill scores at the lower wind speed bins and overall negative WN skill scores at higher wind speed bins.
4) Downscaling increased negative wind speed biases of input HRRR forecasts at stations located in wind-prone lee-slope

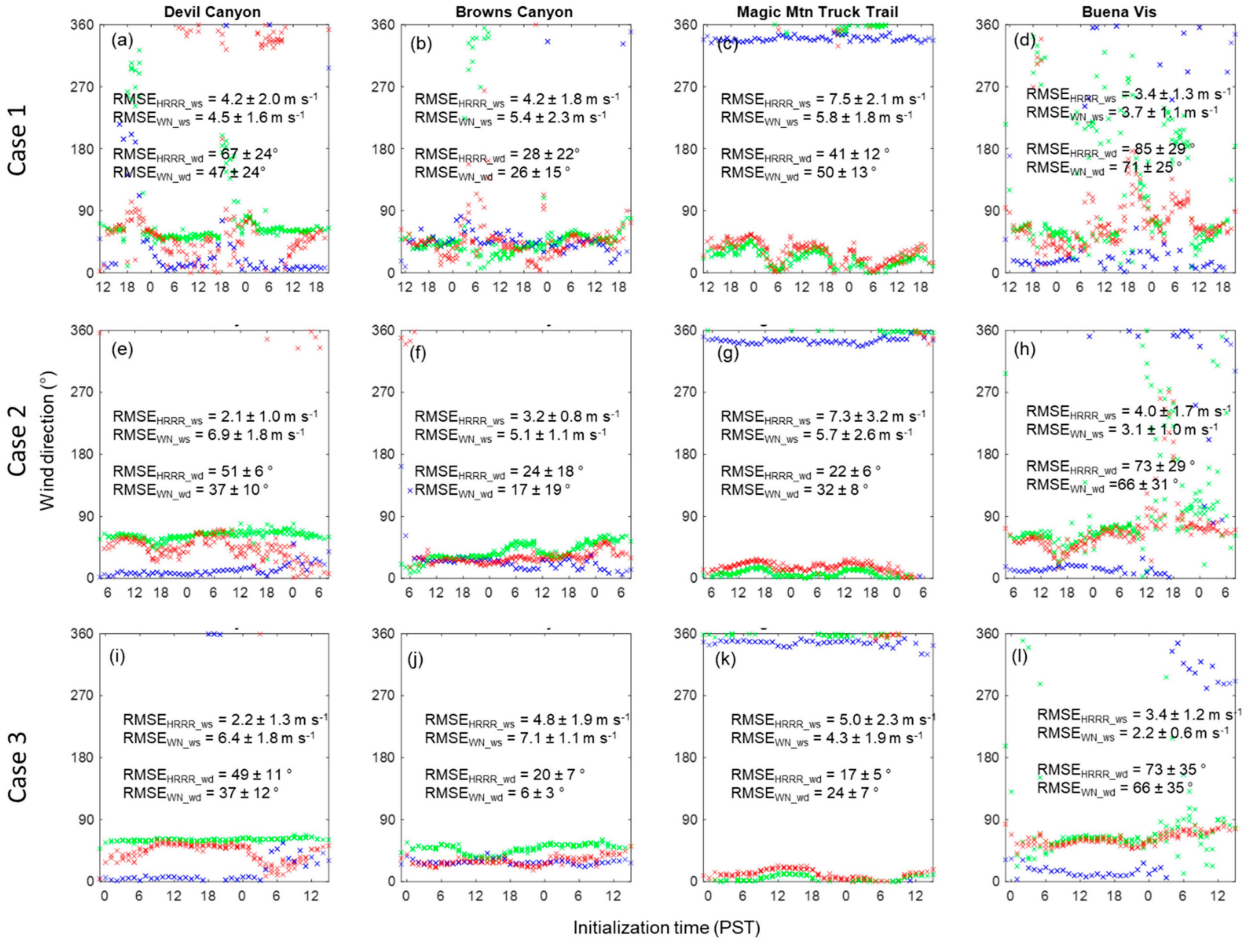

FIG. 16. Time series plots of wind directions (a),(e),(i) Devil Canyon, (b),(f),(j) Browns Canyon, (c),(g),(k) Magic Mountain Track Trail, and (d),(h),(l) Buena Vis stations for the cases 1–3. Observed, HRRR, and WN wind directions are indicated by blue, green, and red, respectively. HRRR and WN RMSE values (mean ± standard deviation) of wind speeds and directions are also shown in each panel. The locations of each station with detailed topography are shown in Figs. S2–S6.

canyons as shown by decreased forecast skill scores and large averaged negative biases. Also, stations located at well-exposed ridgetop sites benefitted from downscaling when the stations had negative input HRRR forecast biases, given that the ridgetops were sufficiently resolved in WN.

5) The lack of treatment of the thermal dynamics driving mountain-wave dynamics is a limitation of WN for downscaling during Santa Ana wind events. Improved modeling of Santa Ana winds will require representation of these driving dynamics at microscale resolutions, including the proper thermal stratification and terrain representation at mountain top height. A gravity wave parameterization such as the one implemented in Gutmann et al. (2016) could potentially be incorporated into WN to improve downscaling during such events.

Few previous studies have evaluated the accuracy of diagnostic wind models over complex terrain under downslope windstorms such as Santa Ana winds. To our knowledge, this is the first study to assess the forecast skill of WN in a complex topographic region under Santa Ana winds. Based on our work, WN with the current approach (mass-conserving option, logarithmic profile initialization) is suited for downscaling gridded HRRR wind speed forecasts in the large Southern California domain. However, users should be aware that WN tends to reduce forecast accuracy in leeward slopes and canyons during downslope windstorm regimes. Further exploration of the dependence of WN simulation accuracy on mesh resolution, atmospheric stability, spatially varying surface roughness, diurnal slope flow parameterization option, and input weather forecast (WRF Model, for example) are some important topics to be investigated in future work.

WN may degrade forecast accuracy of input NWP model forecast on the leeside slopes and canyons during Santa Ana winds. As a result, burned area and fire spread rate may be underestimated on the lee sides of mountain ranges during a high downslope wind event if WN output is used for fire spread modeling. With the present initialization strategy, the conservation of energy and more sophisticated nonneutral stability options may be necessary to improve forecast skill scores on those wind-prone locations during Santa Ana winds and other downslope windstorm events in complex terrain.

Nonetheless, the diagnostic downscaling approach used in WN is a highly efficient tool to downscale forecasts from operational models. A combination of NWP and deep learning may be a potential future alternative avenue (e.g., Le Toumelin et al. 2023).

As a final recommendation to operational users, both of these model systems lack in their ability to adequately capture thermally driven wind phenomena like mountain waves, and that is the biggest caveat. WN does an adequate job representing terrain impacts except on lee slopes but does not currently have the ability to resolve mountain-wave activity and hydraulic jumps that are not assimilated from the input source (e.g., the HRRR). Therefore, large initial errors propagate in lee-slope areas while ridge tops generally see better performance with the WN simulations.

It is generally understood that atmospheric processes such as hydraulic jumps and wave-breaking phenomena can induce high surface wind speeds at various places and times during downslope windstorms. However, penetration of such high winds into lee slope canyons and mountain passes is not well explored. The logarithmic wind profile is generally considered to be a reliable estimator of 10-m wind speed in the surface layer for neutral static stability over flat terrain (Stull 1988), but it may not be well tested in complex terrain, especially during Santa Ana winds (Cao and Fovell 2016). Therefore, it is worth verifying the dependence of WN performance on the model initialization methods (logarithmic or power-law wind profile from the 10-m HRRR winds versus HRRR 3D wind field) in wind-prone lee-slope canyons and mountain passes. These topics invite further investigation.

Acknowledgments. This research was funded by Southern California Edison (Grant SB220035) and the University of California Office of the President Laboratory Fees Program (Grant LFR-20-652467). We thank three anonymous reviewers and Editor in Chief Matt Bunkers for their careful reviews and insightful comments, which were crucial to the improvement of this article.

Data availability statement. The forecast data used in this study are available from Amazon Web Services website (https://noaa-hrrr-bdp-pds.s3.amazonaws.com/index.html). SCE observation data are publicly available via the Meteorological Assimilation Data Ingest System (MADIS; https://madis.ncep.noaa.gov) or Mesowest (https://mesowest.utah.edu).

REFERENCES

Barnes, L. R., E. C. Gruntfest, M. H. Hayden, D. M. Schultz, and C. Benight, 2007: False alarms and close calls: A conceptual model of warning accuracy. *Wea. Forecasting*, **22**, 1140–1147, https://doi.org/10.1175/WAF1031.1.

Barry, R. G., 2008: *Mountain Weather and Climate*. 3rd ed. Cambridge University Press, 262 pp., https://doi.org/10.1017/CBO9780511754753.

Barstad, I., and S. Gronas, 2006: Dynamical structures for southwesterly airflow over southern Norway: The role of dissipation. *Tellus*, **58A**, 2–18, https://doi.org/10.1111/j.1600-0870.2006.00152.x.

Benjamin, S. G., E. P. James, E. J. Szoke, P. T. Schlatter, and J. M. Brown, 2023: The 30 December 2021 Colorado Front Range windstorm and Marshall Fire: Evolution of surface and 3D structure, NWP guidance, NWS forecasts, and decision support. *Wea. Forecasting*, **38**, 2551–2573, https://doi.org/10.1175/WAF-D-23-0086.1.

Cao, Y., and R. G. Fovell, 2016: Downslope windstorms of San Diego County. Part I: A case study. *Mon. Wea. Rev.*, **144**, 529–552, https://doi.org/10.1175/MWR-D-15-0147.1.

——, and ——, 2018: Downslope windstorms of San Diego County. Part II: Physics ensemble analyses and gust forecasting. *Wea. Forecasting*, **33**, 539–559, https://doi.org/10.1175/WAF-D-17-0177.1.

Chow, F. K., S. F. J. De Wekker, and B. J. Snyder, Eds., 2013: *Mountain Weather Research and Forecasting: Recent Progress and Current Challenges*. Springer, 750 pp.

——, C. Schär, N. Ban, K. A. Lundquist, L. Schlemmer, and X. Shi, 2019: Crossing multiple gray zones in the transition from mesoscale to microscale simulation over complex terrain. *Atmosphere*, **10**, 274, https://doi.org/10.3390/atmos10050274.

Dowell, D. C., and Coauthors, 2022: The High-Resolution Rapid Refresh (HRRR): An hourly updating convection-allowing forecast model. Part I: Motivation and system description. *Wea. Forecasting*, **37**, 1371–1395, https://doi.org/10.1175/WAF-D-21-0151.1.

Durran, D. R., 1990: Mountain waves and downslope winds. *Atmospheric Processes over Complex Terrain*, *Meteor. Monogr.*, No. 45, Amer. Meteor. Soc., 59–81, https://doi.org/10.1007/978-1-935704-25-6_4.

——, 2003: Downslope winds. *Encyclopedia of Atmospheric Sciences*, G. North, J. Pyle, and F. Zhang, Eds., Elsevier Science, 644–650.

Forthofer, J. M., B. W. Butler, and N. S. Wagenbrenner, 2014: A comparison of three approaches for simulating fine-scale surface winds in support of wildland fire management. Part I. Model formulation and comparison against measurements. *Int. J. Wildland Fire*, **23**, 969–981, https://doi.org/10.1071/WF12089.

Fosberg, M. A., 1984: A diagnostic three-dimensional mass and momentum conserving wind model for complex terrain. *Proc. Third Conf. on Mountain Meteorology*, Portland, OR, Amer. Meteor. Soc., 13–16.

Fovell, R. G., and A. Gallagher, 2018: Winds and gusts during the Thomas fire. *Fire*, **1**, 47, https://doi.org/10.3390/fire1030047.

Gutmann, E., I. Barstad, M. Clark, J. Arnold, and R. Rasmussen, 2016: The Intermediate Complexity Atmospheric Research model (ICAR). *J. Hydrometeor.*, **17**, 957–973, https://doi.org/10.1175/JHM-D-15-0155.1.

Hersbach, H., and Coauthors, 2020: The ERA5 global reanalysis. *Quart. J. Roy. Meteor. Soc.*, **146**, 1999–2049, https://doi.org/10.1002/qj.3803.

Homicz, G. F., 2002: Three-dimensional wind field modeling: A review. Sandia National Laboratories SAND Rep. 2597, 80 pp., https://doi.org/10.2172/801406.

Hughes, M. R., and A. Hall, 2010: Local and synoptic mechanisms causing Southern California's Santa Ana winds. *Climate Dyn.*, **34**, 847–857, https://doi.org/10.1007/s00382-009-0650-4.

Jones, C., F. Fujioka, and L. M. V. Carvalho, 2010: Forecast skill of synoptic conditions associated with Santa Ana winds in Southern California. *Mon. Wea. Rev.*, **138**, 4528–4541, https://doi.org/10.1175/2010MWR3406.1.

Le Toumelin, L., I. Gouttevin, N. Helbig, C. Galiez, M. Roux, and F. Karbou, 2023: Emulating the adaptation of wind fields

to complex terrain with deep learning. *Artif. Intell. Earth Syst.*, **2**, e220034, https://doi.org/10.1175/AIES-D-22-0034.1.

Mahrt, L., 1982: Momentum balance of gravity flows. *J. Atmos. Sci.*, **39**, 2701–2711, https://doi.org/10.1175/1520-0469(1982)039<2701:MBOGF>2.0.CO;2.

Moritz, M. A., T. J. Moody, M. A. Krawchuk, M. Hughes, and A. Hall, 2010: Spatial variation in extreme winds predicts large wildfire locations in chaparral ecosystems. *Geophys. Res. Lett.*, **37**, L04801, https://doi.org/10.1029/2009GL041735.

Onishi, G., 1969: A numerical method for three-dimensional mountain waves. *J. Meteor. Soc. Japan*, **47**, 353–359.

Raphael, M. N., 2003: The Santa Ana winds of California. *Earth Interact.*, **7**, https://doi.org/10.1175/1087-3562(2003)007<0001:TSAWOC>2.0.CO;2.

Rolinski, T., S. B. Capps, and W. Zhuang, 2019: Santa Ana winds: A descriptive climatology. *Wea. Forecasting*, **34**, 257–275, https://doi.org/10.1175/WAF-D-18-0160.1.

Schaefer, J. T., 1990: The critical success index as an indicator of warning skill. *Wea. Forecasting*, **5**, 570–575, https://doi.org/10.1175/1520-0434(1990)005<0570:TCSIAA>2.0.CO;2.

Siuta, D., G. West, and R. Stull, 2017: WRF hub-height wind forecast sensitivity to PBL scheme, grid length, and initial condition choice in complex terrain. *Wea. Forecasting*, **32**, 493–509, https://doi.org/10.1175/WAF-D-16-0120.1.

Stull, R. B., 1988: *An Introduction to Boundary Layer Meteorology*. Kluwer Academic, 666 pp.

——, 2011: *Meteorology for Scientists and Engineers*. 2nd ed. Brooks/Cole, 938 pp.

Sukup, S., 2013: Damaging downslope wind events in the San Gabriel Valley of Southern California. NOAA/NWS Doc., 26 pp., https://www.weather.gov/media/wrh/online_publications/TAs/TA1602.pdf.

Wagenbrenner, N. S., J. M. Forthofer, B. K. Lamb, K. S. Shannon, and B. W. Butler, 2016: Downscaling surface wind predictions from numerical weather prediction models in complex terrain with WindNinja. *Atmos. Chem. Phys.*, **16**, 5229–5241, https://doi.org/10.5194/acp-16-5229-2016.

——, ——, W. G. Page, and B. W. Butler, 2019: Development and evaluation of a Reynolds-Averaged Navier–Stokes solver in WindNinja for operational wildland fire applications. *Atmosphere*, **10**, 672, https://doi.org/10.3390/atmos10110672.

Wilks, D. S., 1995: *Statistical Methods in the Atmospheric Sciences: An Introduction*. Academic Press, 467 pp.

WMO, 2017: *Guidelines for Nowcasting Techniques*. WMO, 82 pp.